Available online at www.sciencedirect.com
ScienceDirect
Infrared Physics & Technology 51 (2008) 495–504
INFRARED PHYSICS & TECHNOLOGY
www.elsevier.com/locate/infrared

The IR antenna pair coupled sensor element and its potential application in wavefront sensing

Weidong Yang [a], Michael C. Roggemann [a,*], Kyle Cooper [b], William Buller [b], Nikola Subotic [b], Christopher Middlebrook [a], Glenn D. Boreman [c]

[a] *ECE Department, Michigan Technological University, Houghton, MI 49931, USA*
[b] *Michigan Tech Research Institute, Ann Arbor, MI 48105, USA*
[c] *Center for Research and Education in Optics and Lasers, University of Central Florida, Orlando, FL 32816, USA*

Received 25 June 2007
Available online 26 January 2008

Abstract

A single IR antenna-coupled square-law sensor does not preserve the phase of the radiation field. We considered an IR radiation detector element in which the square-law sensor is coupled with a pair of IR dipole antennas, the simplest coherently interconnected IR antenna array with the potential of preserving phase information. The circuit equivalent model is employed for analyzing the response features of an element to a tilted incident plane wave. The analytical results show that the response of such an element contains the phase difference information of incident radiation field at the positions of the two antennas and can be characterized by its induced phase shift, Δ, and the "visibility" of its oscillation profile, κ. In addition, the numerical computations for the case of shifted square-law detectors shows that Δ and κ are strongly affected by, and therefore can be controlled by the electric and geometrical parameters of the antenna element system. Furthermore, a method of using the response measurement of such elements to retrieve the wavefront phase information is also provided.

PACS: 07.57.−c; 07.57.Kp

Keywords: Phased infrared antenna array; Infrared antenna pair coupled detectors; Phase measurement; Infrared detector

0. Introduction

IR sensors coupled with IR antennas provide a unique infrared detection technique. Unlike the traditional IR detection technology, the antenna-coupled radiation detection technique separates the radiation collection from the radiation sensing, and therefore it may outperform conventional IR sensors since the sensing element in such a device can be fabricated at sub-wavelength scales, and therefore its response time to the radiation can be greatly reduced, while its radiation collection ability is retained. Since the antenna is used as the radiation collection component, such a device will be capable of good polarization and wavelength selectivity. Furthermore, the antennas could be arranged to work coherently in the form of an array with the potential of providing new optical remote sensing and imaging techniques.

Various single antenna-coupled sensors have been extensively studied [1–7]. Fabrication and performance studies of antenna-coupled sensor arrays also have been reported [8–12]. However, since these arrays are formed by isolated single antenna-coupled sensors for imaging applications, or are formed by sensors connected in series for the purpose of response enhancement, the elements of the arrays do not preserve any phase information.

In this paper, we study a simple, but coherently operating IR antenna array element: a dipole antenna pair

* Corresponding author. Tel.: +1 906 487 2164; fax: +1 906 487 2949.
E-mail address: mroggema@mtu.edu (M.C. Roggemann).

1350-4495/$ - see front matter © 2008 Elsevier B.V. All rights reserved.
doi:10.1016/j.infrared.2007.11.004

coupled sensor unit. In the first section, the configuration of such an element and its equivalent-circuit model are introduced. In the second section, the response features of such an element to the phase difference of the incident field are analyzed. Based on some key parameters measured by other researchers [13], the relations between these features and the electric and geometrical parameters of the system are analyzed numerically. In the third section, the validity of an application of such elements in wavefront sensing is discussed.

1. Model of a single antenna pair

The IR antenna pair element under study in this paper consists of a pair of IR dipoles, coplanar striplines, and a square-law sensor, which is bolometer in this paper, as shown in Fig. 1. The IR dipoles collect the radiation at two different positions. The coplanar striplines guide the IR waves and connect the dipoles. The sensor converts the energy transferred by the striplines into heat which causes electrical changes in the bolometer which can be measured electronically. In practice, these elements are typically fabricated on a dielectric substrate.

In order to give a simple but insightful description of the voltage/current wave propagation in the system, circuit theory is employed and the element shown in Fig. 1 is converted into an equivalent circuit as illustrated in Fig. 2, in which the antenna and the bolometer are described by lumped circuits and the coplanar striplines are described by transmission lines. The antennas on the left and the right are characterized by their corresponding output impedances, Z_{a1} and Z_{a2}, and the radiation induced voltages, V_{a1} and V_{a2}. The bolometer is characterized by its impedance Z_b which is real. The transmission lines on the left and right are characterized by their characteristic impedances Z_{01} and Z_{02}, their propagation factors γ_1 and γ_2, and their physical lengths L_1 and L_2, respectively.

In general, the parameters on each side of the bolometer need not be identical. In this paper, the detector element is called a balanced antenna pair element (BAPE) if the parameters are symmetric. Otherwise, it is called an unbalanced antenna pair element (UAPE). It should be noted that our discussions throughout this paper are limited to the cases of using identical antennas even in the UAPEs.

The response to the radiation field is measured by the voltage in the readout electronics (not shown in figures). The voltage readout from the bolometer is linearly proportional to its temperature change, which is also linearly proportional to the power dissipated on it [14]. Hence, in the following sections of this paper, the power P that is dissipated in the bolometer will be used to represent the response of the element. P is calculated from

$$P = \frac{1}{2} \cdot Z_b \cdot |I|^2, \tag{1}$$

where I is the induced current.

Further detailed calculations based on the transmission line theory and linear superposition theory of the voltage/current waves in the circuits show that the current going through the bolometer can generally be expressed as

$$I = A_1 \cdot V_{a1} + A_2 \cdot V_{a2}, \tag{2}$$

where the coefficient A_1 and A_2 are completely determined by the parameters of the dipole pair system. The analytical expressions for A_1 and A_2 can be found in the Appendix. For BAPEs, $A_1 = A_2$ and the current can be expressed as

$$I_{\mathrm{BAPE}} = A \cdot (V_{a1} + V_{a2}). \tag{3}$$

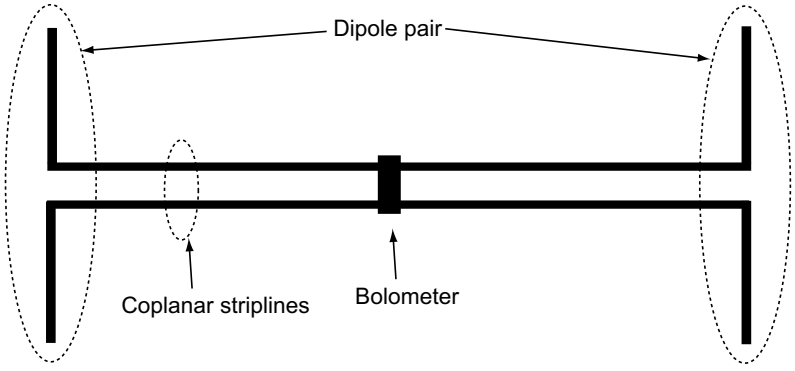

Fig. 1. Graphic illustration of dipole antenna pair system.

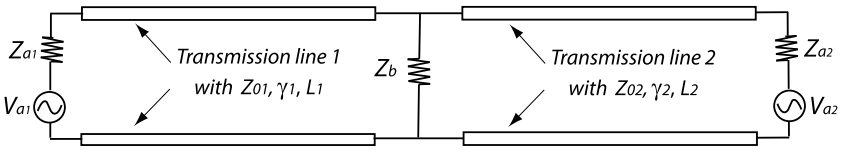

Fig. 2. Graphic illustration of equivalent circuit for the dipole antenna pair system in Fig. 1.

Since transmission line theory is employed in the circuit equivalent model as described in Fig. 2, the mutual coupling effect between the two dipoles has automatically been included in the analysis.

2. Response of the BAPE and UAPE to the phase difference of the incident field

2.1. General case

Consider the case in which the complex field at the locations of the dipoles have the same amplitude but different phase, such as would be the case for a tilted plane wave falling on the plane containing the dipoles. In this case

$$V_{a1} = V_{a2} \cdot e^{i\phi}, \tag{4}$$

where ϕ is the phase difference between V_{a1} and V_{a2}.

Using Eqs. (1), (3), and (4) the response of BAPEs to the phase difference ϕ can be written as

$$P_{\mathrm{BAPE}} = P^0_{\mathrm{BAPE}} \cdot [1 + \cos(\phi)], \tag{5}$$

where $P^0_{\mathrm{BAPE}} = Z_b \cdot |AV_{a2}|^2$.

For the UAPEs, let $A_1/A_2 = a \cdot \exp\{i\Delta\}$ where a and Δ are the modulus and phase angle of the complex number A_1/A_2, then the response of the UAPEs can generally be written as:

$$P_{\mathrm{UAPE}} = P^0_{\mathrm{UAPE}} \cdot [1 + \kappa \cdot \cos(\phi + \Delta)], \tag{6}$$

where $P^0_{\mathrm{UAPE}} = Z_b \cdot (1 + a^2)|A_2V_{a2}|^2/2$ and $\kappa = 2a/(1 + a^2)$ which is the "visibility" of the oscillation with respective to ϕ.

From the Appendix, it can be seen that A_1 and A_2 are determined only by the parameters of the transmission lines and various impedances which are constants with respect to the angle of incidence of radiation field, and therefore the resulting a, Δ and κ are also constants. Since $|V_{a2}|^2$ or $|V_{a1}|^2$ are proportional to the associated single antenna response pattern, one can see that P^0_{BAPE} and P^0_{UAPE} are also proportional to the associated antenna response pattern that is generally symmetric, but is a function of angle of incidence of the radiation wavefront [15]. Thus, it can be seen that the response pattern of a BAPE or UAPE is a single antenna response pattern modulated by an oscillation factor of ϕ that can be characterized by an induced phase shift Δ and a visibility κ.

2.2. UAPEs with shifted bolometer

As can be seen in the last section, the antenna pair coupled sensor element can not only record the phase difference ϕ of the incident field, but can also apply a phase shift Δ to the response measurement. This is an important feature for the potential applications of such elements in wavefront sensing and beam formation. Using a numerical analysis method we now study the dependence of Δ and κ on the attenuation constant and the antenna spacing. For the UAPE, we examine the case in which the imbalance of the parameters is caused by shifting the bolometer from the center of the dipoles, potentially a simple way to make an UAPE.

In the following computations, the data published in [13] is used to obtain estimates of the key physical parameters. In Ref. [13] the following values were obtained at resonance: $Z_{a1} = Z_{a2} = 50\,\Omega$, effective index $n_{\mathrm{eff}} = 1.7$ for $\lambda_0 = 10.6\,\mu\mathrm{m}$, and three attenuation constants $\alpha = (0.18, 0.35, 0.58)\,\mu\mathrm{m}^{-1}$ and their corresponding characteristic impedances $Z_0 = Z_{01} = Z_{02} = (102, 133, 160)\Omega$ were chosen. In addition, $Z_b = 50\,\Omega$ was chosen according to the profiles of P^0_{BAPE} vs. Z_b for the three group values of (Z_0, α) as shown in Fig. 3 so that the responses are close to their maximums. It should be noted that the specific values of the Z_b does not affect the ratio A_1/A_2 and as a consequence does not affect the values of Δ and κ because Z_b affects the reflection/transmission rate of the waves from either of the two antennas by the same factor.

2.2.1. The Δ, κ, and $P^0_{\mathrm{UAPE}}/P^0_{\mathrm{BAPE}}$ for half-wave spaced UAPEs

In general, the induced phase shift Δ, visibility κ and relative strength of response $P^0_{\mathrm{UAPE}}/P^0_{\mathrm{BAPE}}$ are functions of both the bolometer shifting distance δ, and the spacing between dipoles d. In this subsection, for convenience in observing the effect of the bolometer shifting distance δ, a half-wave spaced UAPE is used for computation in which the spacing d between the dipoles is fixed at $d = \lambda/2$. Figs. 4–6 show the relation curves of the Δ, κ, and $P^0_{\mathrm{UAPE}}/P^0_{\mathrm{BAPE}}$ with the shifting distance δ of the bolometer correspondingly.

Fig. 4 shows that the induced phase shift does not follow exactly the relationship of $\Delta = 2 \cdot 2\pi \cdot \delta/\lambda_{\mathrm{eff}}$ due to the complexity of the interference of the waves at the bolometer when the attenuation effect is finite. However, the curve with the higher attenuation constant (dotted line) is closer to the curve for $\Delta = 2 \cdot 2\pi \cdot \delta/\lambda_{\mathrm{eff}}$ (dash-dotted line), in which the higher attenuation reduces more of the multiple reflection waves between the antenna and the bolometer.

Fig. 5 shows that the visibility of the responses is the best $(\kappa = 1)$ when the bolometer is on the center of the dipole pair and the visibility will be reduced when the bolometer is shifted closer to one of the dipoles. The reduction in visibility is proportional to the amount of attenuation.

Fig. 6 shows that the relative response strength, $P^0_{\mathrm{UAPE}}/P^0_{\mathrm{BAPE}}$, will increase with increasing shift distance δ. This is a result of the bolometer receiving more signal as its position is shifted closer to one of the dipoles. For lower attenuation cases, the signal it receives does not vary much with the shifted distance, as shown by the solid line.

2.2.2. The Δ and κ for UAPEs with large spacing

In the preceding section, it was shown that the induced phase shift, in general, is not linearly proportional to the bolometer shift distance when the dipole spacing is a half wavelength. In this section, it will be shown that such

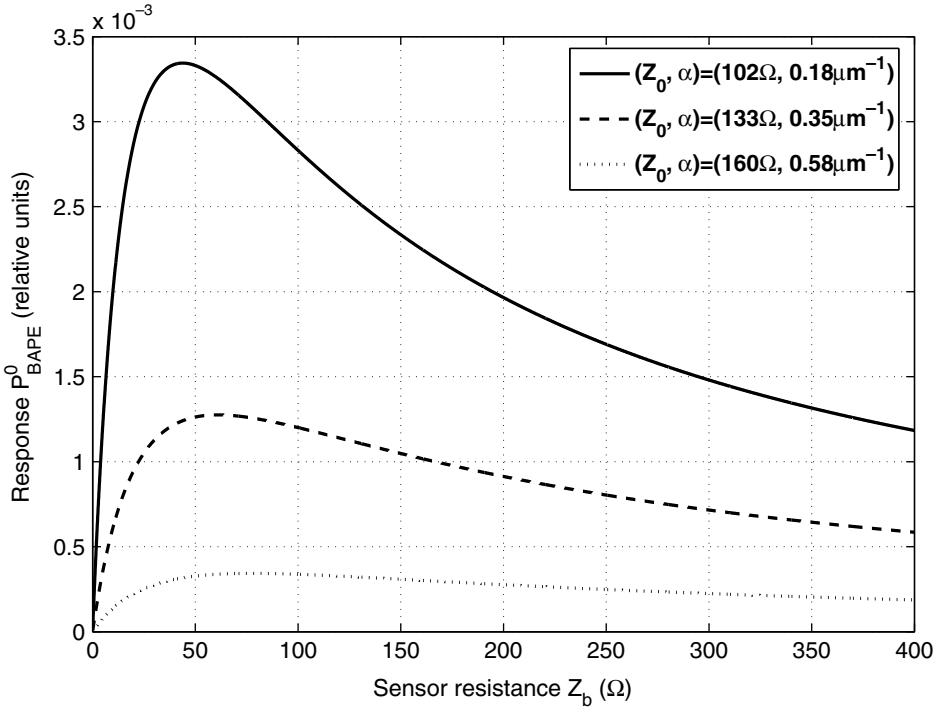

Fig. 3. The relative responses of half-wave spacing BAPE to the sensor resistance. The relative units of the response is for the values when the stimulated voltage amplitude is set to 1.

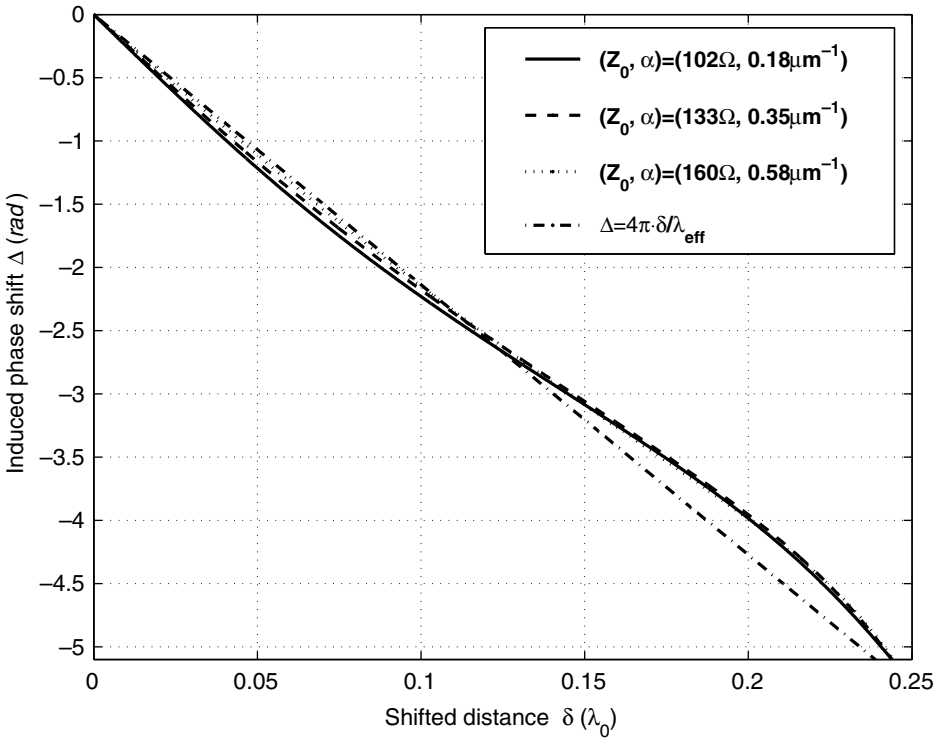

Fig. 4. The induced phase shift Δ vs. bolometer shift distance δ.

complex relationships can approach more simple forms for antenna pairs with larger spacing. For convenience, the bolometer shift distance is fixed at $\delta = 0.0735\lambda_0 = 0.779$ μm, the distance at which a phase shift of $\pi/2$ would be expected if a simple linear relationship of $\Delta = 2 \cdot 2\pi \cdot \delta/\lambda_{\text{eff}}$ were used.

Fig. 7 shows that under the three attenuation constants considered, the induced phase shift approaches to $\pi/2$, a

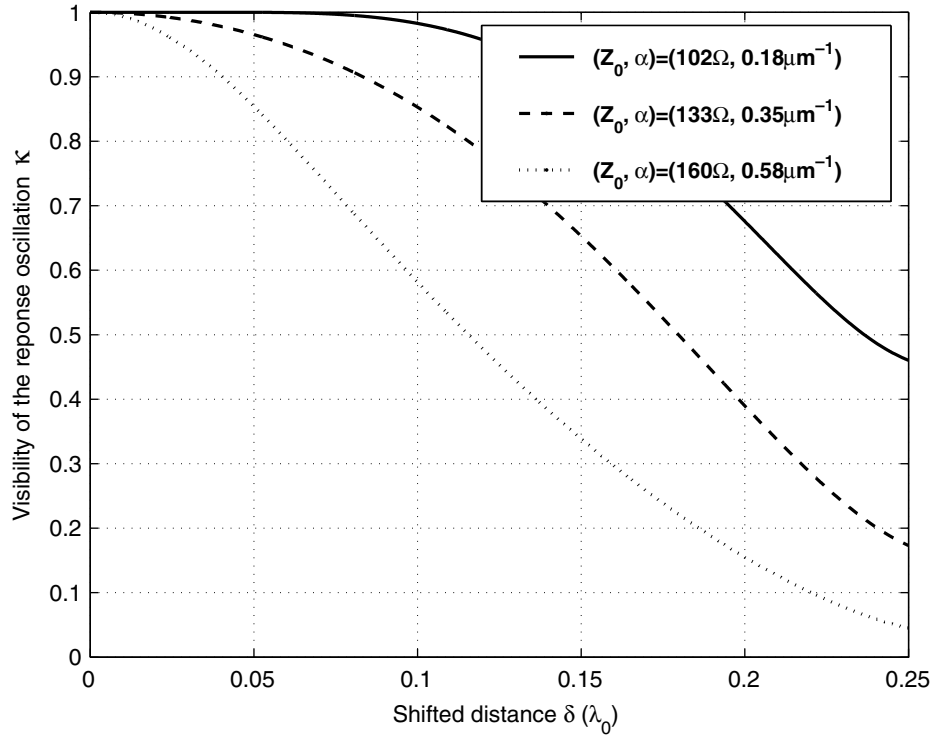

Fig. 5. The response visibility κ vs. bolometer shift distance δ.

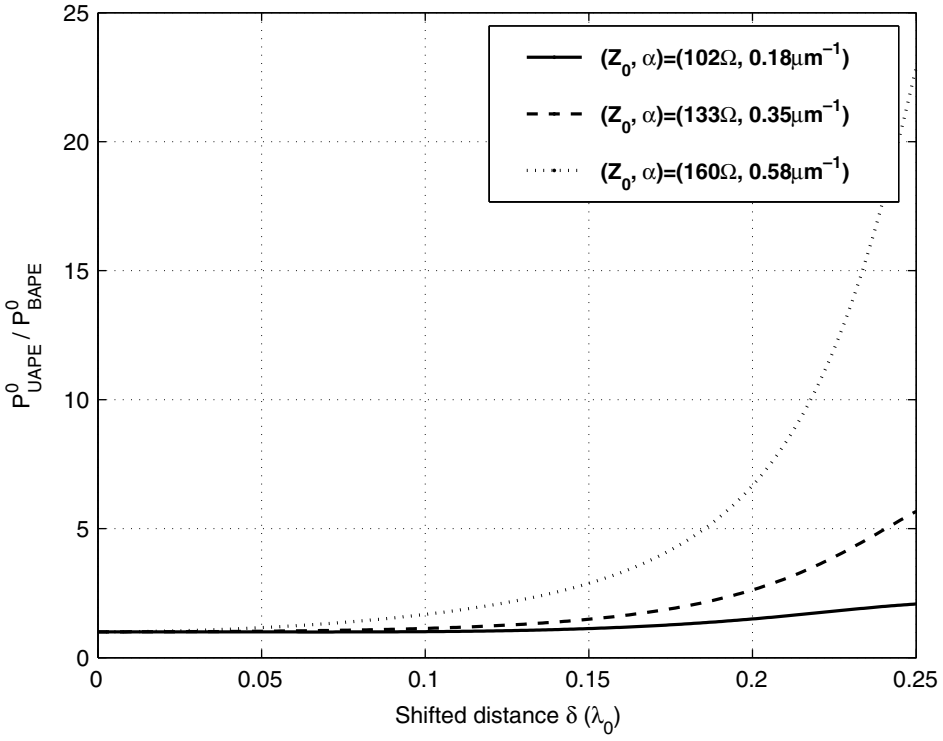

Fig. 6. Relative response strength $P^0_{\mathrm{UAPE}}/P^0_{\mathrm{BAPE}}$ vs. bolometer shift distance δ.

constant determined by the $\Delta = 2 \cdot 2\pi \cdot \delta/\lambda_{\mathrm{eff}}$ as the dipole spacing increases. The cases with higher attenuation approach this constant at smaller values of d.

The visibility of the response is shown in Fig. 8 for the cases where the separation is larger. As the spacing gets larger, the visibility can be approximated by the results of

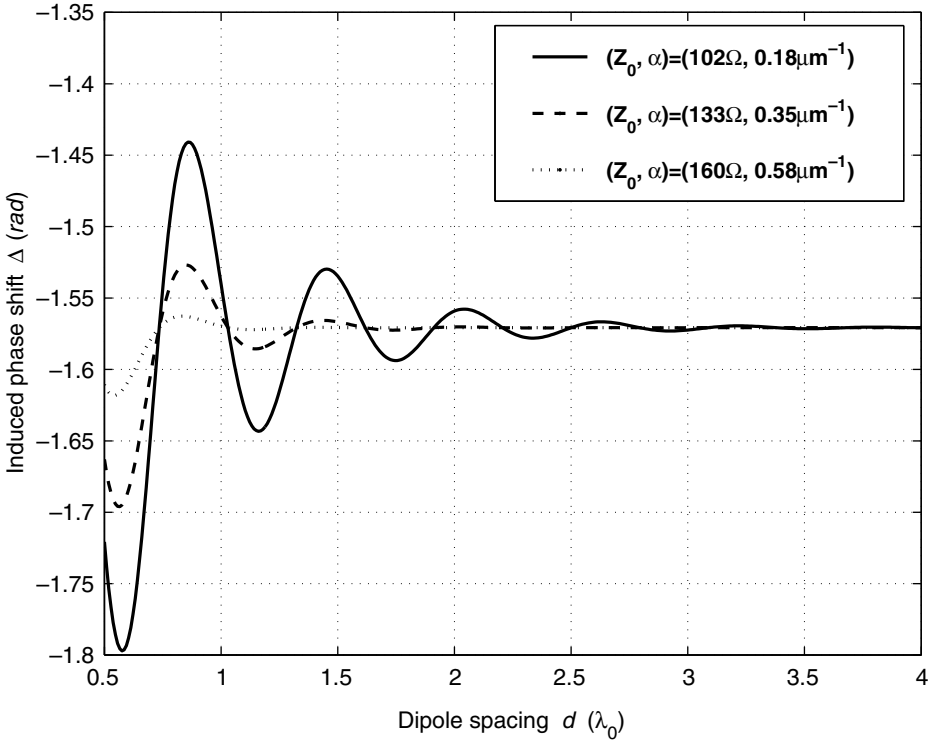

Fig. 7. The induced phase shift Δ vs. dipole spacing d.

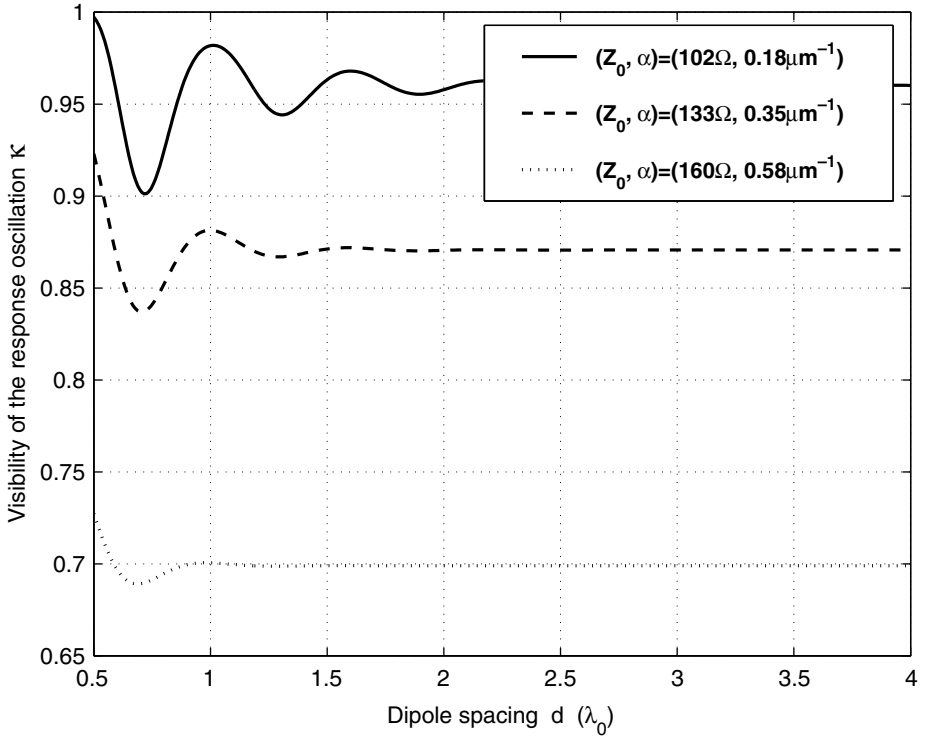

Fig. 8. The response visibility κ vs. dipole spacing d.

simple superposition of two evanescent waves from the two dipoles: $\kappa = 2 \cdot \exp(2 \cdot \delta\alpha)/[1 + \exp(4 \cdot \delta\alpha)]$. For cases of $\alpha = 0.18, 0.35, 0.58\ \mu m^{-1}$ in this example, their corresponding visibilities approach 0.96, 0.87 and 0.70, respectively.

It is evident that the finite attenuation constant of the transmission lines will keep the multiple reflections of the waves between the dipole and bolometer, and generate some complexity in the Δ and κ of the response. Qualita-

tively, the complexity can be reduced and approximated by the results of only the simple superposition of two evanescent waves from the dipoles, when the attenuation is high and the dipole spacing is large enough so that the distance between bolometer and closest dipole is greater than the attenuation length $\sim 1/\alpha$, which means

$$\alpha \cdot \left(\frac{d}{2} - \delta\right) \gg 1. \tag{7}$$

Under this condition, the multiple reflection of the waves between the bolometer and dipoles can be ignored, and the following approximation is obtained:

$$\Delta \approx 4\pi \cdot \frac{\delta}{\lambda_{\text{eff}}}, \tag{8}$$

$$\kappa \approx \frac{2 \cdot e^{2\delta\alpha}}{1 + e^{4\delta\alpha}}. \tag{9}$$

3. Resolving the angle of incidence of local wavefront by UAPEs: an application example

We now describe a simple method of resolving the angle of incidence of the local wavefront based on the measurements provided by an UAPE.

Consider one measurement of the response of one UAPE to a IR field, say, a plane wave falling on the device with angle of incidence θ as shown in Panel (a) of Fig. 9. Such a field will generate a phase difference ϕ at the two dipole positions in which $\phi(\theta) = 2\pi \cdot d \cdot \sin(\theta)/\lambda$. Based on Eq. (6), a direct measurement of the response will give

$$P_1(\theta) = P_0(\theta) \cdot \{1 + \kappa \cdot \cos[\phi(\theta) + \Delta]\}, \tag{10}$$

where $P_0(\theta)$ is the shortened form of P^0_{UAPE} and is proportional to the antenna response pattern as described in Section 2.1.

If this UAPE is rotated by $\pm 180°$ so that the two dipoles can exchange their spatial position as shown in Panel (b) of Fig. 9, the angular response pattern of the UAPE must also flip and the new response measurement $P_2(\theta)$ on this rotated UAPE must be $P_2(\theta) = P_1(-\theta) = P_0(-\theta) \cdot \{1 + \kappa \cdot \cos[\phi(-\theta) + \Delta]\}$. Since the antenna response pattern is even with $P_0(-\theta) = P_0(\theta)$ and $\phi(\theta)$ is odd with $\phi(-\theta) = -\phi(\theta)$, the $P_2(\theta)$ can be expressed as the following:

$$P_2(\theta) = P_0(\theta) \cdot \{1 + \kappa \cdot \cos[\phi(\theta) - \Delta]\}. \tag{11}$$

If the UAPE has been designed to have $\Delta = \pi/2$, Eqs. (10) and (11) will be $P_1(\theta) = P_0(\theta) \cdot \{1 - \kappa \cdot \sin[\phi(\theta)]\}$ and $P_2(\theta) = P_0(\theta) \cdot \{1 + \kappa \cdot \sin[\phi(\theta)]\}$ respectively. Further processing these two measurements will lead to a solution for the phase difference $\phi(\theta) \in (-\pi/2, \pi/2)$ and the single antenna pattern $P_0(\theta)$:

$$\phi(\theta) = \arcsin[\kappa^{-1} \cdot P_r(\theta)], \tag{12}$$

$$P_0(\theta) = \frac{P_1(\theta) + P_2(\theta)}{2}, \tag{13}$$

where $P_r(\theta)$ is defined as $P_r(\theta) \equiv [P_2(\theta) - P_1(\theta)]/[P_2(\theta) + P_1(\theta)]$. It can be seen that the phase difference ϕ that is within the region of $(-\pi/2, \pi/2)$ can be resolved by appropriate processing the two measurements using the same UAPEs, regardless of the specific forms of angular response patterns of the dipoles. Additionally, the local incident angle θ of the radiation field can be obtained by using the geometrical relation $\phi(\theta) = 2\pi \cdot d \cdot \sin(\theta)/\lambda$, and the retrieved angle θ_r can be expressed as

$$\theta_r = \arcsin\left[\frac{\lambda}{2\pi \cdot d} \cdot \arcsin(\kappa^{-1} \cdot P_r)\right], \tag{14}$$

where θ_r may range over $(-\pi/2, \pi/2)$. However, it should be noted that since the phase difference ϕ is calculated using Eq. (12) and it is limited to $-\pi/2 \leqslant \phi \leqslant \pi/2$, as a result angle of incident can be correctly estimated only when $\theta \in (-\arcsin[\lambda/(4d)], \arcsin[\lambda/(4d)])$ for cases of $d \geqslant \lambda/4$. For example, for the case of $d = \lambda/4$, the two measurements can be used to calculate the angle of incidence within $(-\pi/2, \pi/2)$; while for the case of $d = \lambda/2$, the two measurements can be used to calculate the angle of incidence within $(-\pi/6, \pi/6)$ only. Nevertheless, Eqs. (12) and (14) indicate that the UAPE with $\Delta = \pi/2$ can be used for wavefront sensing.

To illustrate the effectiveness of the UAPEs in sensing the angle of incidence of a wavefront, a half-wave spaced UAPE is used as an example and the results of processing the angular patterns of P_1 and P_2 are shown in Fig. 10. In the calculation, this half-wave UAPE is assumed to have

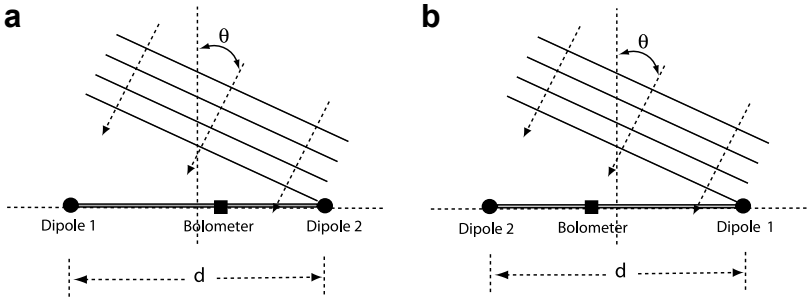

Fig. 9. An UAPE in an incident wave field before and after the rotation. (a) An UAPE in an incident wave. (b) The flipped UAPE in the same wave.

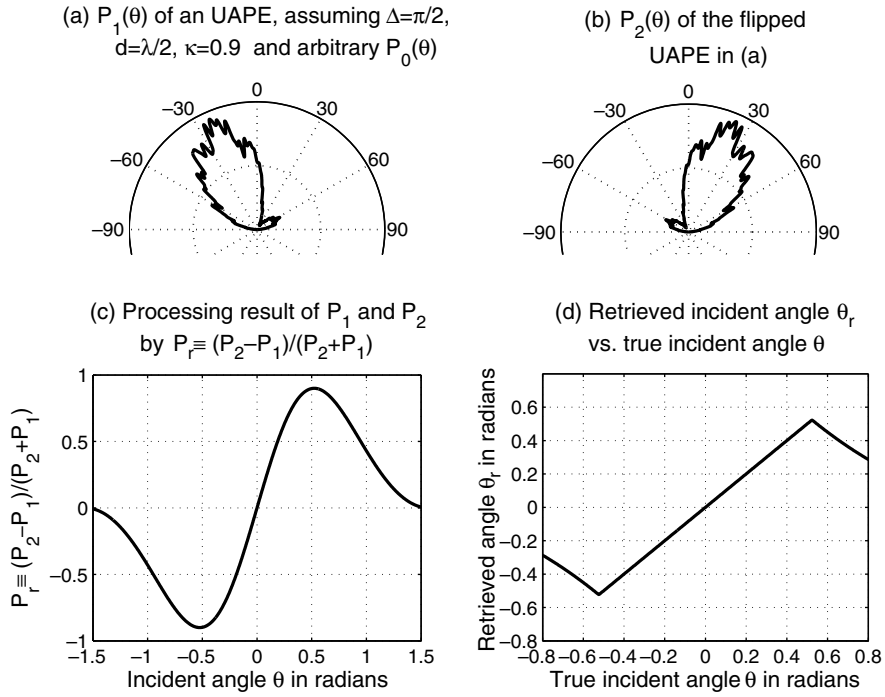

Fig. 10. Illustration of the method of obtaining the local wave incident angle θ by appropriate processing the two measurements on the case of a half-wave spaced UAPE with $\Delta = \pi/2$.

$\Delta = \pi/2$, $d = \lambda/2$, $\kappa = 0.9$ and an *arbitrary* $P_0(\theta)$. The response pattern of the whole UAPE is calculated based on Eq. (10) and is shown in Panel (a) while the response pattern of the rotated UAPE is calculated based on Eq. (11) and is shown in Panel (b). The random fluctuations in signal on the two patterns are from the arbitrary $P_0(\theta)$ and are used to show the independence of the processing results with specific form of $P_0(\theta)$. Panel (c) shows the result of processing the two patterns in (a) and (b) by $(P_2 - P_1)/(P_2 + P_1)$. It can be seen that this processing avoids dealing with the complexity of single antenna pattern $P_0(\theta)$ and generates an odd function which indicates a monotonic relation with the incident angle within the region of $(-\pi/6, \pi/6)$. Panel (d) shows that the retrieved incident angle θ_r according to Eq. (14) matches with the true incident angle θ within the range of $\theta \in (-\pi/6, \pi/6)$, as indicated by the 45° straight line segment within that region.

In practice, spatially shifted bolometers may be used to realize $\Delta = \pm\pi/2$. In addition, instead of rotating one UAPE manually and performing the measurement separately, two UAPEs with opposite sign of Δ can be fabricated on the same substrate and hence the P_1 and P_2 can be measured simultaneously. It can be expected that such a local wavefront measuring method by UAPE pairs can be extended to the cases of measuring the wavefront at multiple spacial locations, and thus the wavefront function of the radiation field can be eventually reconstructed [16]. The detailed discussion on this aspect is beyond the scope of this paper and is not presented here.

4. Conclusion

In this paper, a dipole antenna pair coupled IR sensor model has been introduced, and the phase-preserving response behaviors have been analyzed based on a equivalent circuit model. The results show that, in general, the response of such an IR sensor can be characterized by the induced phase shift Δ and the response visibility κ. The response features of the UAPE with shifted bolometers were studied numerically, using physical parameters obtained by previous work. Due to multiple reflections of the evanescent waves within the short distances between the dipole and the bolometer, the complexity of the Δ and κ features with respect to the attenuation constant α, bolometer shifting distance δ, and dipole spacing d should be taken into account in designing such devices, except when the bolometer is far enough from the dipoles compared to the attenuation length. In addition, a method of estimating the phase difference ϕ, and consequently the angle of incidence θ of a wavefront by processing the response measurements of UAPE-pairs has also been introduced. The validity of this method shows that the UAPE's could be applied to further development of on-chip IR wavefront sensing technology.

Acknowledgements

Authors wish to thank the Defense Advanced Research Projects Agency and the Air Force office of Scientific Research, Contract No. FA 9550-05-1-0404.

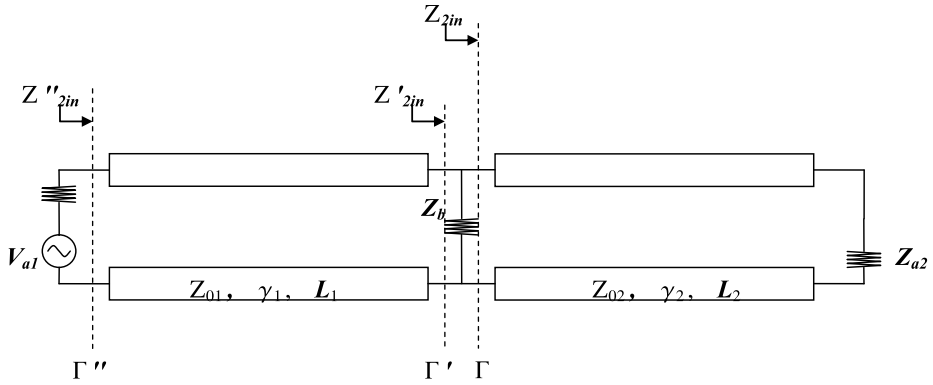

Fig. 11. Graphic illustration of the equivalent circuits used for analyzing the voltage/current contribution from the source V_{a1}.

Appendix

The voltage/current wave on the bolometer is the linear superposition of the waves from the sources of V_{a1} and V_{a2} according to Thevenin's Theorem. The voltage/current wave from the source V_{a1} is calculated based on the analysis shown in Fig. 11.

The input impedances for the circuits on the right of each reference planes of Γ, Γ' and Γ'' are noted as $Z_{2\text{in}}$, $Z'_{2\text{in}}$ and $Z''_{2\text{in}}$ correspondingly and can be expressed as:

$$Z_{2\text{in}} = Z_{02} \cdot \frac{Z_{a2}\cosh(\gamma_2 L_2) + Z_{02}\sinh(\gamma_2 L_2)}{Z_{02}\cosh(\gamma_2 L_2) + Z_{a2}\sinh(\gamma_2 L_2)}, \tag{15}$$

$$Z'_{2\text{in}} = \frac{Z_b Z_{2\text{in}}}{Z_b + Z_{2\text{in}}}, \tag{16}$$

$$Z''_{2\text{in}} = Z_{01} \cdot \frac{Z'_{2\text{in}}\cosh(\gamma_1 L_1) + Z_{01}\sinh(\gamma_1 L_1)}{Z_{01}\cosh(\gamma_1 L_1) + Z'_{2\text{in}}\sinh(\gamma_1 L_1)}. \tag{17}$$

According to the transmission line theory, the voltage and current waves on the transmission line between plane Γ' and Γ'' can be described as $V(x) = V^+ \cdot \exp\{\gamma_1 \cdot x\} + V^- \cdot \exp\{-\gamma_1 \cdot x\}$ and $I(x) = V^+/Z_{01} \cdot \exp\{\gamma_1 \cdot x\} - V^-/Z_{01} \cdot \exp\{-\gamma_1 \cdot x\}$ where x denotes the coordinate of an arbitrary point on the transmission line relative to the plane Γ', V^+ and V^- denote the coefficients of voltage waves propagating along $\pm x$ directions. Since the current $I(-L_1)$ and voltage $V(-L_1)$ on port of plane Γ'' are $I(-L_1) = V_{a1}/(Z''_{2\text{in}} + Z_{a1})$ and $V(-L_1) = Z''_{2\text{in}} \cdot V_{a1}/(Z''_{2\text{in}} + Z_{a1})$, the coefficients V^+ and V^- can thus be determined and the voltage on port of plane Γ' is $V(x=0) = V^+ + V^- = V_{a1} \cdot [Z''_{2\text{in}}\cosh(\gamma_1 L_1) - Z_{01}\sinh(\gamma_1 L_1)]/(Z_{a1} + Z''_{2\text{in}})$. Therefore, the coefficient A_1 in Eq. (2) is

$$A_1 = \frac{[Z''_{2\text{in}}\cosh(\gamma_1 L_1) - Z_{01}\sinh(\gamma_1 L_1)]}{Z_b(Z_{a1} + Z''_{2\text{in}})}. \tag{18}$$

The voltage/current wave contributed from the source V_{a2} can be analyzed in the same manner and the coefficient A_2 in Eq. (2) can be determined as

$$A_2 = \frac{[Z''_{1\text{in}}\cosh(\gamma_2 L_2) - Z_{02}\sinh(\gamma_2 L_2)]}{Z_b(Z_{a2} + Z''_{1\text{in}})} \tag{19}$$

in which

$$Z''_{1\text{in}} = Z_{02} \cdot \frac{Z'_{1\text{in}}\cosh(\gamma_2 L_2) + Z_{02}\sinh(\gamma_2 L_2)}{Z_{02}\cosh(\gamma_2 L_2) + Z'_{1\text{in}}\sinh(\gamma_2 L_2)} \tag{20}$$

with

$$Z'_{1\text{in}} = \frac{Z_b Z_{1\text{in}}}{Z_b + Z_{1\text{in}}}, \tag{21}$$

$$Z_{1\text{in}} = Z_{01} \cdot \frac{Z_{a1}\cosh(\gamma_1 L_1) + Z_{01}\sinh(\gamma_1 L_1)}{Z_{01}\cosh(\gamma_1 L_1) + Z_{a1}\sinh(\gamma_1 L_1)}. \tag{22}$$

References

[1] R. Comptin, R. McPhedran, Z. Popovic, G. Rebeiz, P. Tong, D. Rutledge, Bow-tie antennas on a dielectric half-space: theory and experiment, IEEE Trans. Antennas Propag. 35 (1987) 622–631.
[2] E.N. Grossman, J.E. Sauvageau, D.G. McDonald, Lithographic spiral antennas at short wavelengths, Appl. Phys. Lett. 59 (1991) 3225–3227.
[3] I. Wilke, W. Herrmann, F.K. Kneubühl, Integrated nanostrip dipole antennas for coherent 30 THz infrared radiation, Appl. Phys. B 58 (1994) 87–95.
[4] C. Karadi, J. Jauhar, L. Kouwenhoven, K. Wald, P. McEuen, Y. Nagamune, H. Sakaki, Dynamic response of a quantum point contact, J. Opt. Soc. Am. B 11 (1994) 2566–2571.
[5] N. Chong, H. Ahmed, Antenna-coupled polycrystalline silicon air-bridge thermal detector for mid-infrared radiation, Appl. Phys. Lett. 71 (1997) 1607–1609.
[6] C. Fumeaux, W. Herrmann, F.K. Kneubühl, H. Rothuizen, Nanometer thin-film Ni–NiO–Ni diodes for detection and mixing of 30 THz radiation, Infrared Phys. Technol. 39 (1998) 123–183.
[7] I. Codreanu, C. Fumeaus, D.F. Spencer, G.D. Boreman, Microstrop antenna-coupled infrared detector, Electron. Lett. 35 (1999) 2166–2167.
[8] F.J. González, M.A. Gritz, C. Fumeaux, G.D. Boreman, Two dimensional array of antenna-coupled microbolometers, Int. J. Infrared Milli. Waves 23 (2002) 785–797.
[9] F.J. González, C.S. Ashley, P.G. Clem, G.D. Boreman, Antenna-coupled microbolometer arrays with aerogel thermal isolation, Infrared Phys. Technol. 45 (2004) 47–51.
[10] G.D. Boreman, A. Dogariu, C. Christodoulou, D. Kotter, Modulation transfer function of antenna-coupled infrared detector arrays, Appl. Opt. 35 (1996) 6110–6114.
[11] M. Abdel-Rahman, B. Lail, G.D. Boreman, Dual-band millimeter-wave/infrared focalplane arrays, Microw. Opt. Technol. Lett. 46 (2005) 78–80.

[12] F.J. González, J.L. Porter, G.D. Boreman, Antenna-coupled infrared focal plane array, Microw. Opt. Technol. Lett. 48 (2006) 165–166.
[13] T. Mandviwala, B. Lail, G. Boreman, Infrared-frequency coplanar striplines: design, fabrication, and measurements, Microw. Opt. Technol. Lett. 47 (2005) 17–20.
[14] R.H. Kingston, Detection of optical and infrared radiation, in: Springer Series in Optical Science, vol. 10, New York, 1978.
[15] D.B. Rutledge, M.S. Muha, Imaging Antenna Arrays, IEEE Trans. Antenna Propag. 30 (1982) 535–540.
[16] D.C. Ghiglia, M.D. Pritt, Two-Dimensional Phase Unwrapping: Theory Algorithms and Software, Wiley-Interscience Publication, John Wiley & Sons Inc., 1998.